PLOS ONE

RESEARCH ARTICLE

Intrathecal catheter implantation decreases cerebrospinal fluid dynamics in cynomolgus monkeys

Mohammadreza Khani[1,2], Audrey Q. Fu[3], Joshua Pluid[1], Christina P. Gibbs[1], John N. Oshinski[4], Tao Xing[5], Gregory R. Stewart[2,6], Jillynne R. Zeller[7], Bryn A. Martin[1,2]*

1 Department of Chemical and Biological Engineering, University of Idaho, Moscow, ID, United States of America, **2** Alcyone Therapeutics, Lowell, MA, United States of America, **3** Department of Statistical Science, University of Idaho, Moscow, ID, United States of America, **4** Department of Radiology and Imaging Sciences, Emory University, Atlanta, GA, United States of America, **5** Department of Mechanical Engineering, University of Idaho, Moscow, ID, United States of America, **6** Voyager Therapeutics, Cambridge, MA, United States of America, **7** Northern Biomedical Research, Spring Lake, MI, United States of America

* brynm@uidaho.edu

Citation: Khani M, Fu AQ, Pluid J, Gibbs CP, Oshinski JN, Xing T, et al. (2020) Intrathecal catheter implantation decreases cerebrospinal fluid dynamics in cynomolgus monkeys. PLoS ONE 15(12): e0244090. https://doi.org/10.1371/journal.pone.0244090

Editor: Quan Jiang, Henry Ford Health System, UNITED STATES

Received: August 25, 2020

Accepted: December 2, 2020

Published: December 30, 2020

Data Availability Statement: All relevant data are within the paper and its Supporting Information files.

Funding: This work was supported by Voyager Therapeutics, National Institutes of Health, National Institute of General Medical Sciences grant P20GM103408 and 4U54GM104944-04 and the University of Idaho, Vandal Ideas Project. Publication of this article was funded by the University of Idaho Open Access Publishing Fund. The funders had no role in study data collection

Abstract

A detailed understanding of the CSF dynamics is needed for design and optimization of intrathecal drug delivery devices, drugs, and protocols. Preclinical research using large-animal models is important to help define drug pharmacokinetics-pharmacodynamics and safety. In this study, we investigated the impact of catheter implantation in the sub-dural space on CSF flow dynamics in Cynomolgus monkeys. Magnetic resonance imaging (MRI) was performed before and after catheter implantation to quantify the differences based on catheter placement location in the cervical compared to the lumbar spine. Several geometric and hydrodynamic parameters were calculated based on the 3D segmentation and flow analysis. Hagen-Poiseuille equation was used to investigate the impact of catheter implantation on flow reduction and hydraulic resistance. A linear mixed-effects model was used in this study to investigate if there was a statistically significant difference between cervical and lumbar implantation, or between two MRI time points. Results showed that geometric parameters did not change statistically across MRI measurement time points and did not depend on catheter location. However, catheter insertion did have a significant impact on the hydrodynamic parameters and the effect was greater with cervical implantation compared to lumbar implantation. CSF flow rate decreased up to 55% with the catheter located in the cervical region. The maximum flow rate reduction in the lumbar implantation group was 21%. Overall, lumbar catheter implantation disrupted CSF dynamics to a lesser degree than cervical catheter implantation and this effect remained up to two weeks post-catheter implantation in Cynomolgus monkeys.

and analysis, decision to publish, or preparation of the manuscript. Voyager Therapeutics had a role in the study design. Authors BAM and GRS are employed by Alcyone Therapeutics. GRS was employed by Voyager Therapeutics during the course of this study. Alcyone Therapeutics provided support in the form of salary for authors BAM and GRS, but did not have any additional role in the study design, data collection and analysis, decision to publish, or preparation of the manuscript. Voyager Therapeutics provided support in the form of salary for author GRS. Author JRZ is employed by Northern Biomedical Research. Northern Biomedical Research provided support in the form of salary for author JRZ, but did not have any additional role in the study design, data collection and analysis, decision to publish, or preparation of the manuscript. The specific roles of these authors are articulated in the 'author contributions' section.

Competing interests: I have read the journal's policy and the authors of this manuscript have the following competing interests: This study was funded in part by Voyager Therapeutics. Authors BAM and GRS are employed by Alcyone Therapeutics. GRS was employed by Voyager Therapeutics during the course of this study. JRZ is a fulltime employee of Northern Biomedical. BAM has received grant support from Voyager Therapeutics, Genentech, Alcyone Lifesciences, Biogen, and Minnetronix; BAM is a member of the Neurapheresis Research Consortium. BAM is scientific advisory board member for Alcyone Lifesciences, Chiari and Syringomyelia Foundation, The International Society for Hydrocephalus and CSF Disorders, The International CSF Dynamics Society, and has served as a consultant to Voyager Therapeutics, Praxis Medicines, Roche, SwanBio Therapeutics, CereVasc, Minnetronix, Invicro, Genentech, Medtrad Biosystems, Behavior Imaging, Neurosyntek, and Cerebral Therapeutics. There are no patents, products in development or marketed products to declare. This does not alter our adherence to PLOS ONE policies on sharing data and materials.

Background and introduction

A detailed understanding of cerebrospinal fluid (CSF) dynamics is needed for design and optimization of intrathecal drug delivery devices, drugs, and protocols. The intrathecal space, also termed the dural sac, is an anatomic region located between the spinal cord tissue and the dura mater that is filled with CSF. In intrathecal drug delivery, medications are introduced directly to the CSF using a drug delivery system. The most prevalent method of intrathecal drug administration is the externalized intrathecal catheter [1]. One advantage of intrathecal drug delivery is that a lower dose of medication is often possible to administer compared to medication taken orally and fewer medication side effects may be reported. Also, intrathecal drug delivery to the CSF effectively bypasses the blood-brain-barrier thereby allowing delivery of many medications that are typically too large to cross into the brain via systemic drug delivery.

Currently approved medications for intrathecal administration by the U.S. Food and Drug Administration (FDA) include morphine, ziconotide, and baclofen. If the motivation for treatment is to decrease spasticity in body extremities, then the intrathecal catheter can be implanted in the rostral intrathecal space to potentially improve drug spread uniformity across the neuroaxis [2]. Intrathecal drug delivery has been investigated for treatment of lymphoma [3], leptomeningeal cancer [4], and spinal muscular atrophy [3]. Lastly, specialized intrathecal catheters have been implanted to help remove unwanted toxins from the CSF such as blood post-subarachnoid hemorrhage [5, 6] or fungal pathogens in cryptococcal meningitis [7].

Preclinical intrathecal drug delivery studies need to be performed using large-animal models (e.g., monkeys, dogs and sheep) since these models have utility to define drug pharmacokinetic-pharmacodynamics and provide an important tool for assessment of drug safety. Preclinical studies also provide insight into the potential mechanisms of intrathecal drug delivery. Cynomolgus monkeys are a commonly used model for these studies because of their similarity to humans with regard to the pathophysiology of a variety of diseases and presumed similarity with regard to central nervous system anatomy and CSF hydrodynamics.

Unfortunately, we do not know how prolonged intrathecal catheter implantation in nonhuman primates (NHP) or humans may impact CSF dynamics. This is important because the dynamic movement of CSF impacts drug spread along the neuroaxis [8, 9]. Also, it should be noted that CSF dynamics are complex and include a) the net movement of CSF due to production and absorption throughout the CSF system [10], and b) the oscillatory movement of CSF due to cardiac related [11, 12] and respiratory related [13, 14] pressure fluctuations within the CSF system. Concerning item a, the net movement of CSF via analysis of concentration of chemicals over time during intrathecal anesthetic delivery has been analyzed in cynomolgus monkeys [15], baboons [16], and chimpanzees [17]. These chemical concentrations have been studied over various time-frames ranging from 90 minutes to 72 hours, and longer [18, 19]. However, the measurement methods applied in these studies did not allow quantification of cardiac-related CSF oscillations (item b above). For example, if presence of an intrathecal catheter decreases CSF oscillations, neuroaxis drug transport has been predicted to decrease [20].

To our knowledge, no studies have investigated how catheter placement may impact cardiac-related CSF dynamics in Cynomolgus monkeys, or any other species. Our previous study developed a quantitative method to characterize CSF dynamics and geometry in non-human primates (NHPs) using a non-invasive MRI-based protocol [21]. This method was demonstrated to reliably measure CSF dynamics parameters over a two-week period in a group of eight NHPs. The goal of the current study was to apply the same MRI protocol and post-processing methods on a series of scans collected for the same cohort of NHPs to quantify: a) alterations in cardiac-related CSF dynamics due to catheter placement in the intrathecal space, b)

track these changes over time, and c) determine if there are any differences that occur based on catheter implantation location in the cervical compared to lumbar spine.

Materials and methods

Ethics statement

This study was submitted to and approved by the local governing Institutional Animal Care and Use Committee at Northern Biomedical Research (IACUC approval #084-014A, Spring Lake, MI). This study did not unnecessarily duplicate previous experiments and alternatives to the use of live animals were considered. Procedures used in this study were designed with consideration of the well-being of the animals.

Husbandry and animal welfare

This study complied with all applicable sections of the current version (at the time of study 2016) of the Final Rules of the Animal Welfare Act Regulations (9 CFR), and the Guide for the Care and Use of Laboratory Animals, Institute of Laboratory Animal Resources, Commission on Life Sciences, National Research Council, 8th edition. The animals were housed individually in stainless steel cages. The housing was in compliance with the Guide for the Care and Use of Laboratory Animals, DHHS, (NIH) No. 86–23, and the Animal Welfare Act (9 CFR 3). Non-contact absorbent wood chips were used to line the pans underneath the animal's cage. Room temperatures was maintained at 74˚ ± 10˚F. Twenty-five biscuits of PMI Certified Primate Diet #5048 were placed in the feeders daily during the study. More biscuits were provided based on the weight and caloric needs of the animal. Filtered municipal water (City of Norton Shores) was supplied ad libitum via an automatic watering system. All animals in the study were provided with environmental enrichment according to the facility Program of Animal Care that was accredited by the Association for Assessment and Accreditation of Laboratory Animal Care. All animals were observed for morbidity, mortality, injury, and availability of food and water at least twice daily.

Surgery and surgical recovery

For catheter implantation, the animals were pretreated with atropine sulfate as a subcutaneous injection at a dose of 0.04 mg/kg. At least 15 minutes later, an intramuscular dose of 8 mg/kg of ketamine HCl was provided to induce sedation. The animals were masked, intubated, and maintained on approximately 1 liter/min of oxygen and approximately 2.0% isoflurane. The anesthetic gases and mixtures were varied as required by the animal and recorded in the raw data. Prednisolone sodium succinate IV, 30 mg/kg, and flunixin meglumine intramuscular, 2 mg/kg, were administered prior to surgery. A hemilaminectomy was made in the L5 vertebra, the catheter tip was inserted and advanced intrathecally with the tip located near T12/L1 or C5. All of the catheters were terminated in a subcutaneous access port (ClearPort Min, Access Technologies). The actual location of the catheters and catheter tips were verified by a myelogram with Iopamidol. Upon recovery from anesthesia, the animals were provided 0.05 mg/kg intramuscular butorphanol tartrate for analgesia and placed on 5.0 mg/kg post-surgical antibiotic ceftiofur sodium (one injection prior to surgery followed by three injections). A post-surgical recovery period of at least 10 days was taken prior to CSF flow imaging. Following this MRI study, animals were returned to the facility stock colony.

Table 1. Cynomolgus monkey case information.

Designation	Gender	Catheter Placement	Weight (kg)	Age (yr.)
NHP 01	M	C5	4.0	4.1
NHP 02	F	C5	3.3	4.7
NHP 03	F	L1	5.1	4.5
NHP 04	F	L1	3.2	4.4
NHP 05	F	C5	4.8	4.2
NHP 06	F	C5	3.0	4.9
NHP 07	F	L1	4.2	5.2
NHP 08	F	L1	5.8	4.4

https://doi.org/10.1371/journal.pone.0244090.t001

Catheter placement and parameters

Eight (NHP 01–08) healthy cynomolgus monkeys (Macaca fascicularis, origin Mauritius) were obtained from Charles River Research Models, Houston TX with an average weight of 4.4 ± 1.2 kg and age of 4.6 ± 0.4 years (mean ± standard deviation) (Table 1). NHP 01 was male and all other NHPs were female (02–08). These animals were purpose-bred and experimentally naïve.

Each NHP was scanned with an identical MRI protocol (see MRI methods) across all study time points (Fig 1). $MRI_{PRE\text{-}1}$ and $MRI_{PRE\text{-}2}$ were spaced 14 days apart prior to catheter placement. $MRI_{PRE\text{-}1}$ and $MRI_{PRE\text{-}2}$ were used in our previous publication [21] to quantify reliability of CSF flow parameters. At day 17, the NHP's were randomly assigned to have intrathecal catheter implantation (IT-PEPU-35, SAI Infusion Technologies, Lake Villa, IL, U.S.A.) in the spinal subarachnoid space (SAS) at C5 (Cervical Group, n = 4) or L1 (Lumbar Group, n = 4). The catheter had the following dimensions: first 10 cm distal to the tip (ID = 0.38 mm and OD = 0.99 mm), next 24 cm (ID = 1.19 mm and OD = 1.98 mm) and last ~1.5 cm (ID = 1.07 mm and OD = 1.93 mm). Fluoroscopic imaging with contrast agent was used to assist with catheter implantation. On the 24^{th} and 28^{th} days, catheter patency was confirmed through a visual inspection and ability to withdraw CSF from the catheter port. $MRI_{POST\text{-}1}$ was collected on day 31 to study the acute impact of implantation on CSF dynamics and geometry by comparison of results to $MRI_{PRE\text{-}2}$. $MRI_{POST\text{-}2}$ was collected at day 45 to determine if the impact persisted after catheter implantation.

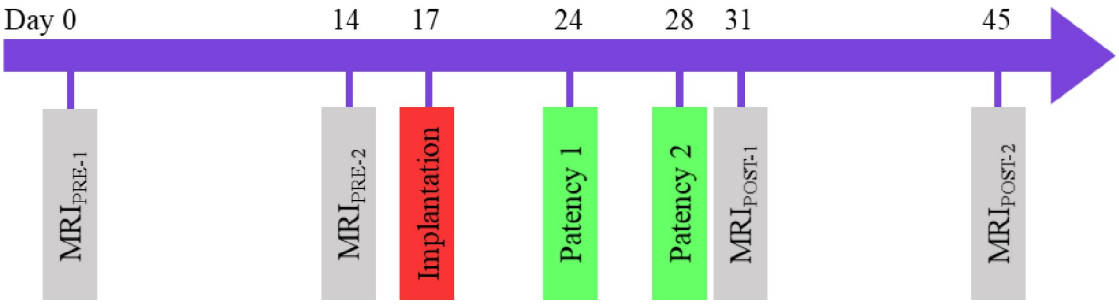

Fig 1. Study outline. This study involved a total of four MRI scans collected over a period of 45 days. $MRI_{PRE\text{-}1}$ and $MRI_{PRE\text{-}2}$ were performed prior to catheter implantation to confirm scan consistency (see results published in Khani et al. [21]). An intrathecal catheter was implanted within the cervical SAS (C5, n = 4) and lumbar SAS (L1, n = 4). Catheter patency was confirmed on day 24 and 28. $MRI_{POST\text{-}1}$ was collected to determine the acute impact of catheter implantation compared to $MRI_{PRE\text{-}2}$. $MRI_{POST\text{-}2}$ was collected to determine if the impact persisted two weeks after implantation.

https://doi.org/10.1371/journal.pone.0244090.g001

MRI scan protocols

MRI scan protocols were previously described in detail by Khani et al. [21]. In brief, all MRI measurements were acquired at Northern Biomedical Research (Norton Shores, Michigan, U.S.A.) on a Philips 3T scanner (Achieva, software V2.6.3.7, Best, The Netherlands). Prior to MRI scanning each NHP was prepared using standard procedures and precautions. NHPs were positioned in the scanner in the supine position without assistance from artificial respiration. During each scan, heart rate and respiration were monitored continuously with ~ 1 liter/minute of oxygen and 1–3% isoflurane anesthetic administered via an endotracheal tube for sedation.

A stack of high-resolution axial T2-weighted MR images of the complete spinal SAS geometry was acquired for each NHP. The anatomical region scanned was ~30 cm in length, which included the intrathecal SAS below the lower brain stem extending caudally to the filum terminale.

Thru-plane (head-foot, z-direction) CSF flow was measured by phase-contrast MRI (PC-MRI) images collected at six axial locations along the spine for each NHP. Axial locations were marked at the foramen magnum (FM), C2-C3, C5-C6, T4-T5, T10-T11, and L3-L4. The slice location for each scan was oriented roughly perpendicular to the CSF flow direction with slice planes intersecting vertebral discs (**Fig 2**).

Image segmentation and flow analysis

The high-resolution T2-weighted anatomic MRI images were semi-automatically segmented using the free open-source ITK-snap software (Version 3.0.0, University of Pennsylvania, U.S.A.) [22], which provided semi-automatic segmentation using active contour methods, as well as manual delineation and image navigation (**Fig 2A**). Frequent use of the manual segmentation tool was utilized in order to view the three orthogonal planes. The catheter was considered to be an empty region within the spinal SAS, because it was not possible to consistently identify within the MR images due to its small lumen diameter. Once the segmentation was complete, the 3D model (**Fig 2B**) was exported in a stereo lithography format for subsequent analysis.

CSF flow was quantified at six axial locations along the spine (**Fig 2C**) using GTFLOW software (64-bit, Version 2.2.10, Gyrotools, Zurich, Switzerland) by the segmentation procedure previously described by Khani et al. [21]. The six distinct flow rates were smoothed in a spatial-temporal fashion using MATLAB and a 2D "fit" function with the fit-type designated as "smoothing-spline". Since heart rate variability was present between the PC-MRI scans, the CSF flow waveform timing was normalized to the average heart rate for all NHPs. An average spatial-temporal CSF waveform was determined for each case. CSF pulse wave velocity, PWV, was computed based on the slope of the arrival time of peak CSF flow along the spine [23].

Geometric and hydrodynamic parameter quantification

Several geometric and hydrodynamic parameters were calculated based on the 3D segmentation and flow analysis using our previously published methods [21]. Total SAS surface area, SA_{sas}, was calculated as the sum of the surface area of spinal cord, SA_c, and dura, SA_d. MR images were unable to specify the small spinal cord nerve root features. Thus, surface area calculations only included surface area of the spinal cord and did not include nerve roots. The total volume of the SAS, V_{sas}, was computed by subtracting the volume of the spinal cord, V_c from the volume of the dura, V_d. Total SAS length, L_{sas}, from the FM to the SAS termination was quantified.

Axial distribution of the SAS cross-sectional area, $A_{sas}(z)$, was based on cross-sectional area of the spinal cord at that location, $A_c(z)$, and dura, $A_d(z)$. The axial distribution of the catheter

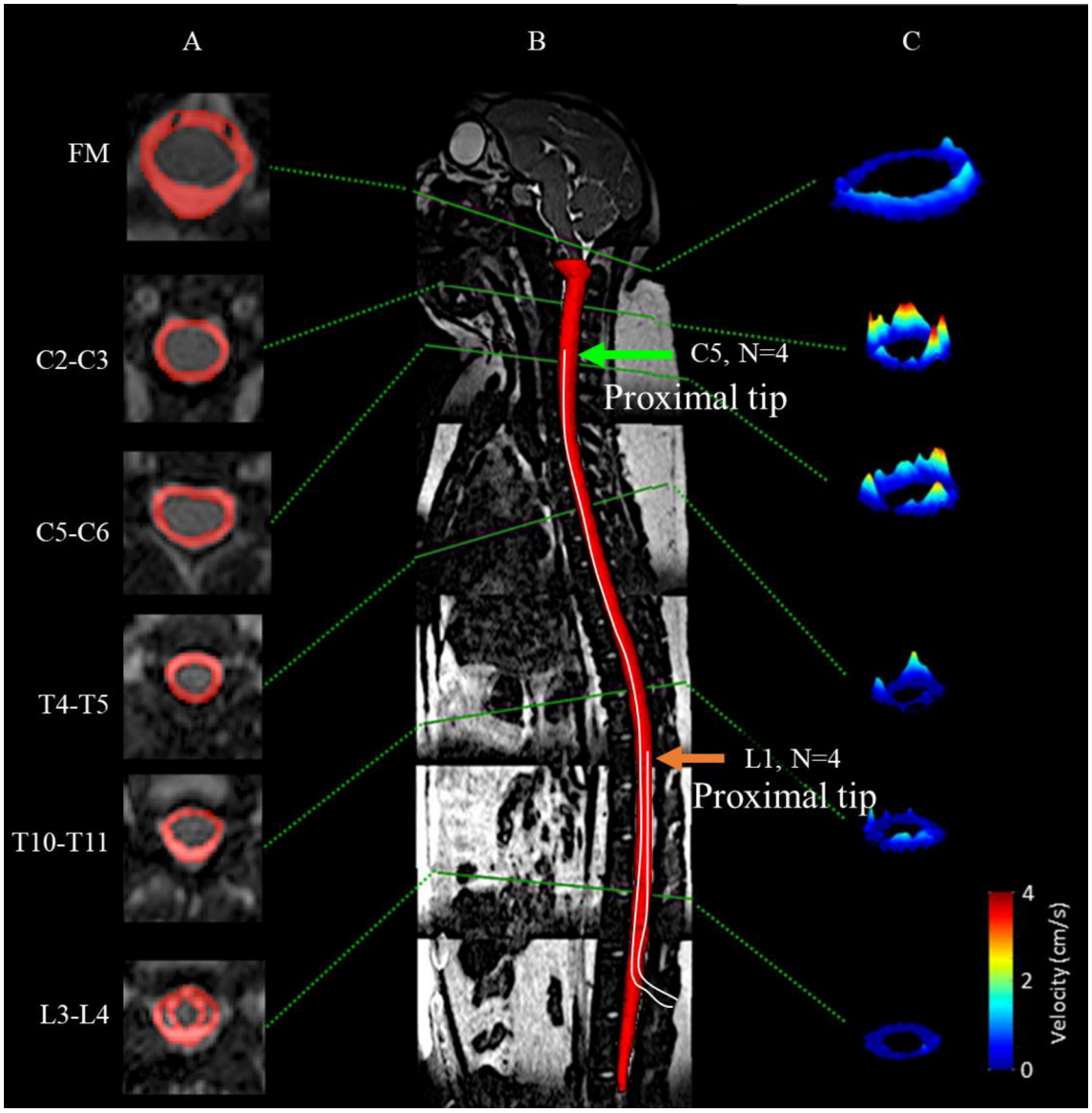

Fig 2. Manual segmentation of the spinal SAS using a T2-weighted MR image. Axial PC-MRI and CSF velocity profiles are indicated at corresponding vertebral levels for a representative cynomolgus monkey analyzed in this study. (A) Visualization of SAS area manually selected around the spinal cord at multiple axial levels. (B) Mid-sagittal high-resolution T2-weighted MRI and 3D visualization of entire SAS geometry. (C) 3D visualization of peak systolic CSF velocity profiles based on in vivo PC-MRI measurements at FM, C2-C3, C5-C6, T4-T5, T11-T12, and L3-L4. Arrows represent the location of catheter placement at the cervical (C5) or lumbar (L1) implantation groups (N = 4 NHPs in each group).

https://doi.org/10.1371/journal.pone.0244090.g002

cross-sectional area for the lumbar and cervical catheters were subtracted for $MRI_{POST\text{-}1}$ and $MRI_{POST\text{-}2}$. Similarly, the hydraulic diameter, $D_h(z) = 4A_{sas}(z)/P_{sas}(z)$, was determined based on the wetted perimeter, $P_{sas}(z)$, with the perimeter computed as the sum of the spinal cord, $P_c(z)$, and dura, $P_d(z)$, perimeters at each z-location. The axial distribution of the catheter perimeter for the lumbar and cervical catheters were added for $MRI_{POST\text{-}1}$ and $MRI_{POST\text{-}2}$. Axial distribution of CSF stroke volume was computed as $SV(z) = \int|Q(z,t)|dt$, where $|Q(z,t)|$ was the absolute value [24]. Peak systolic (toward feet) and diastolic (toward the head) CSF flow rate was quantified as $Q_{sys}(z)$ and $Q_{dia}(z)$, while the CSF flow rate amplitude was given by

$Q_a(z) = Q_{dia}(z) - Q_{sys}(z)$. Spatial mean thru-plane velocity at peak systole was computed as $\bar{U}_{sys}(z) = Q_{sys}(z)/A_{sas}(z)$ and at diastole as $\bar{U}_{dia}(z) = Q_{dia}(z)/A_{sas}(z)$.

Reynolds number based on hydraulic diameter was computed as $Re(z) = (\bar{U}_{sys}(z) \cdot D_h(z))/\nu$, where ν was the kinematic viscosity of CSF at body temperature, 0.693 mPa·s [25]. Reynolds number for external flow around nerve roots was quantified as: $Re_{NR} = \bar{U}_{sys} D_{NR}/\nu$ where nerve roots cylinder diameter, D_{NR}, was given by the axial distribution of nerve roots diameters along the spine, ranging from 0.2 to 0.3 mm [26]. Reynolds number based on the Stokes layer thickness, $\delta = \sqrt{2\nu/\omega}$, was calculated as $Re_\delta(z) = (\bar{U}_{sys}(z) \cdot \delta)/\nu$, where ω was the angular velocity ($\omega = 2\pi/T$) of the volume flow waveform with T is the average cardiac cycle time ($T = 0.53$ s). To assess possibility of instabilities in an oscillatory flow around cylinders, Keulegan-Carpenter number was computed as: $K = \bar{U}_{sys} T/D_{NR}$ and the value of beta is given by, $\beta = Re_{NR}/K = D_{NR}^2/\nu T$. Flow instabilities occur for values of $K>2$ under a given β as shown experimentally by Honji (1981) [27] and theoretically by Hall [28].

Womersley number was computed as $\alpha(z) = \frac{D_h(z)}{2}\sqrt{\omega/\nu}$. To allow parameter comparison across NHPs, each parameter's axial distribution for each NHP was normalized to the average L_{sas} measured for all NHPs. After normalization, the mean axial distribution for each parameter was computed for each group (Cervical or Lumbar catheter implantation) at each MRI time point ($MRI_{PRE\text{-}2}$, $MRI_{POST\text{-}1}$ and $MRI_{POST\text{-}2}$).

Catheter implantation could potentially reduce CSF flow due to increased hydraulic resistance. We estimated the potential flow reduction for the cervical and lumbar implantation group by: $flow\ reduction = 1 - (\sum_{z=0}^{z=L_{sas}} 1/D_{h(z)}{}^4 / \sum_{z=0}^{z=L_{sas}} 1/D_{h-w(z)}{}^4)$. Where $D_h(z)$, was the axial distribution of hydraulic diameter for $MRI_{PRE\text{-}2}$, and $D_{h\text{-}w}(z)$, was the predicted hydraulic diameter by taking into account the axial distribution of catheter area and perimeter for the lumbar and cervical groups. This flow reduction prediction is approximated based on the Hagen-Poiseuille equation for steady, incompressible, laminar pipe flow under the assumption that intracranial pressure pulsations, that drive CSF flow along the spine, are not affected by presence or absence of the catheter (i.e. Δp = constant).

Statistical analysis

We hypothesized that implantation of the catheter would decrease CSF dynamics and geometry, and that these changes would be elevated for NHPs with cervical implantation compared to lumbar implantation. For each of the parameters investigated here, MRI measurements were taken at multiple locations along the spinal cord for each cynomolgus monkey. Since the NHPs were randomly selected from a population, we developed the following linear mixed-effects model:

$$y_i = \beta_0 + \beta_1 x_{1i} + \beta_2 x_{1i}^2 + \beta_3 x_{2i} + \beta_4 x_{3i} + \beta_5 x_{4i} + z_{0i} + z_{1i} x_{1i} + z_{2i} x_{1i}^2 + \varepsilon_i$$

y_i represented the geometric or hydrodynamic parameter of interest, x_{1i} stood for the location, while x_{2i} was the catheter location (cervical / lumbar) or the MRI time point (e.g., $MRI_{PRE\text{-}2}$, $MRI_{POST\text{-}1}$ and $MRI_{POST\text{-}2}$), x_{3i} and x_{4i} are the age and weight of each NHP, respectively. The random error, ε_i, has a normal distribution with mean 0 and variance σ^2: $\varepsilon_i \sim N(0, \sigma^2)$. While β are fixed effect sizes, z represent the random-effect coefficients, which follow a

multivariate normal distribution with mean of 0 and a symmetric variance-covariance matrix:

$$\begin{pmatrix} Z_{0i} \\ Z_{1i} \\ Z_{2i} \end{pmatrix} \sim N\left(\begin{pmatrix} 0 \\ 0 \\ 0 \end{pmatrix}, \begin{pmatrix} \sigma_0^2 & \sigma_{01} & \sigma_{02} \\ \sigma_{01} & \sigma_1^2 & \sigma_{12} \\ \sigma_{02} & \sigma_{12} & \sigma_2^2 \end{pmatrix} \right)$$

We used the "*fitlme*" function in Matlab (Ver. R2019a Mathworks Corp., Natick, MA) to estimate the parameters in this linear mixed-effects model and test the hypothesis.

This model treats the catheter location and the MRI time point as a fixed effect, with the corresponding coefficient indicating the effect size. We could further test whether the true effect size is significantly different from zero. If so, it means that there is a statistically significant difference between cervical and lumbar implantation, or between two MRI time points. This model treats the NHPs as random; this means that the multiple measurements from an NHP can form a curve, and that this curve may be different from one NHP to another.

Using this linear mixed-effects model, we estimated the relative effect sizes of the following seven pairs: four pairs comparing time points (time points PRE-2C versus POST-1C for cervical implantation; time points PRE-2L versus POST-1L for lumbar implantation; time points PRE-2C versus POST-2C for cervical implantation; times points PRE-2L versus POST-2L for lumbar implantation), and three comparing cervical versus lumbar implantation (at time point PRE-2, POST-1 and POST-2). For each pair, we tested the statistical significance of the two groups being different and obtained a P value. Since we performed this analysis for 13 geometric and hydrodynamic parameters, we derived 13×7 = 91 P values. Many of these P values were dependent due to the strong dependence among several parameters of interest. We accounted for multiple comparison with Bonferroni correction by adjusting the threshold for P values to be 0.05/91 = 5.49e-4. This identified a highly conservative set of significant P values. Note that this approach assumes independence among P values. When two parameters of interest are highly correlated, they would lead to similar P values that are both identified to be significant after correction. In this case, we can only conclude that one or both parameters are significant, but we cannot pinpoint the truly significant parameter.

Results

A summary of geometric and hydrodynamic parameter results obtained at $MRI_{PRE\text{-}2}$, $MRI_{POST\text{-}1}$, and $MRI_{POST\text{-}2}$ for the cervical (C) and lumbar (L) groups are shown in **Table 2** (Mean ± STD). Statistical assessments revealed that multiple hydrodynamic parameters were statistically different across study groups and time points (**Table 3**). However, geometric parameters were largely unchanged.

Geometric parameter results

Results indicated that cervical catheter insertion altered spinal SAS geometry to a greater degree than lumbar catheter insertion (**Fig 3**). Overall, 33 out of 42 geometric parameters did not change statistically across MRI measurement time points or depending on catheter location (**Table 3**).

Axial distribution of geometric parameters showed relatively small changes across the lumbar and cervical implantation groups for A_d, A_c, A_{sas}, P_d, and P_c at all time points (**Fig 3A–3E**). However, P_{sas} (**Fig 3F**) for the $MRI_{POST\text{-}1C}$ and $MRI_{POST\text{-}2C}$ groups increased significantly below the catheter tip after insertion (**Table 3**). Average CSF volume in the spinal SAS for all NHPs across all measurement time points ($MRI_{PRE\text{-}2}$, MRIPOST$_{\text{-}1}$ and $MRI_{POST\text{-}2}$ for both cervical and lumbar groups) was 7.00 ml. Average cross-sectional area for spinal cord, dura

Table 2. Cynomolgus monkey geometric and hydrodynamic parameter results at each measurement time point and for the cervical and lumbar implantation groups.

Parameters		MRI_{PRE-2C} Mean ± STD		MRI_{PRE-2L} Mean ± STD		$MRI_{POST-1C}$ Mean ± STD		$MRI_{POST-1L}$ Mean ± STD		$MRI_{POST-2C}$ Mean ± STD		$MRI_{POST-2L}$ Mean ± STD	
Geometric parameter (Mean value along spine)	*P_c (mm)*	13.39	2.06	14.06	1.64	13.31	2.10	14.09	1.44	13.79	2.13	14.65	1.20
	P_d (mm)	21.53	1.96	22.30	1.66	21.81	1.91	22.30	1.47	22.05	1.97	22.55	1.38
	P_sas (mm)	35.72	4.38	37.46	3.91	39.29	4.15	38.06	3.08	40.60	4.82	39.02	2.88
	A_c (mm^2)	14.40	2.72	15.47	3.07	14.89	3.25	16.12	2.57	15.46	3.46	16.24	2.25
	A_d (mm^2)	38.21	6.22	40.10	5.89	38.89	6.00	40.05	5.11	39.91	6.05	40.72	4.88
	A_sas (mm^2)	23.81	4.66	24.63	4.31	22.51	4.50	23.76	3.76	22.96	4.17	24.30	3.62
	SA_c (cm^2)	40.24	3.38	42.40	2.71	38.68	1.67	41.32	2.80	39.85	3.43	42.97	1.76
	SA_d (cm^2)	64.85	3.83	67.37	3.54	63.59	4.72	65.55	3.03	63.87	4.90	66.32	2.47
	SA_sas (cm^2)	105.09	7.17	109.78	6.07	102.27	6.12	106.87	5.74	103.72	8.22	109.29	4.22
	V_c (mL)	4.33	0.39	4.70	0.59	4.35	0.41	4.76	0.44	4.48	0.39	4.80	0.32
	V_d (mL)	11.51	1.18	12.13	1.21	11.35	1.10	11.80	0.95	11.59	1.03	12.00	0.87
	V_sas (mL)	7.17	0.82	7.43	0.79	6.57	0.77	6.99	0.57	6.68	0.67	7.15	0.58
Hydrodynamic parameter (Mean value along spine)	*D_h (mm)*	2.67	0.34	2.66	0.37	2.35	0.43	2.54	0.34	2.31	0.29	2.52	0.29
	Re	32.32	14.12	28.51	13.12	15.13	11.74	21.77	11.61	10.79	6.58	21.45	13.03
	α	5.45	0.86	5.43	0.65	4.61	1.04	5.05	0.66	4.42	0.56	5.09	0.59
	U_peak-sys (cm/s)	-0.92	0.42	-0.84	0.36	-0.49	0.40	-0.63	0.32	-0.34	0.21	-0.64	0.39
	U_peak-dia (cm/s)	0.66	0.30	0.56	0.23	0.40	0.29	0.46	0.23	0.32	0.19	0.49	0.26
	Q_peak-sys (mL/s)	-0.21	0.09	-0.19	0.08	-0.11	0.08	-0.15	0.08	-0.08	0.04	-0.15	0.09
	Q_peak-dia (mL/s)	0.15	0.06	0.13	0.05	0.08	0.05	0.11	0.05	0.07	0.04	0.11	0.06
	Q_a (mL/s)	0.36	0.22	0.32	0.25	0.19	0.11	0.25	0.20	0.15	0.08	0.26	0.21
	SV (cm^3)	0.06	0.02	0.05	0.03	0.03	0.02	0.05	0.03	0.03	0.01	0.04	0.03
	PWV (cm/s)	1.15	1.21	1.11	0.21	1.25	0.59	1.16	0.52	1.16	0.06	1.09	0.21

Note: The mean axial distribution for each parameter is shown based on N = 4 NHPs in each group.

https://doi.org/10.1371/journal.pone.0244090.t002

and SAS for all NHPs was 15.43, 39.65 and 23.66 mm^2, respectively. Average perimeter for spinal cord, dura and SAS was 13.88, 22.09, and 38.36 mm, respectively. Average SAS cross-sectional perimeter (Fig 3F) in the thoracic region increased from 3 to 6 mm with cervical catheter implantation.

Hydrodynamic parameter results

Catheter implantation was found to decrease CSF flow pulsations along the entire spine and this impact was greater for cervical catheter implantation compared to lumbar implantation (Fig 4). For example, $MRI_{POST-1C}$ flow rate was lower than MRI_{PRE-2C} for all axial locations. Catheter implantation was found to decrease CSF flow pulsations even 31 days after catheter insertion ($MRI_{POST-2C}$ and $MRI_{POST-2L}$). These findings were supported by statistical analysis that showed changes in hydrodynamic parameters with cervical and lumbar catheter implantation to be highly significant for 40 out of 49 hydrodynamic parameters with p values $< 0.05/91$ (Table 3).

CSF flow rate of each NHP group quantified along the spine had a similar waveform shape, and axial distribution (Fig 4). CSF flow waveform showed a systolic peak at 100 to 150 ms in the cervical spine ranging from 0.2–0.6 (ml/s) for all NHPs. CSF flow rate at the C5-C6 for

Table 3. Statistical comparison of parameters across measurement time points for baseline vs. follow-up MRIs and cervical vs. lumbar catheter insertion. P values are obtained from linear mixed effects model (see "Statistical analysis" section for details).

Parameters		*Baseline vs Follow-up*				*Cervical vs Lumbar*		
		$MRI_{PRE\text{-}2C}$ vs $MRI_{POST\text{-}1C}$	$MRI_{PRE\text{-}2L}$ vs $MRI_{POST\text{-}1L}$	$MRI_{PRE\text{-}2C}$ vs $MRI_{POST\text{-}2C}$	$MRI_{PRE\text{-}2L}$ vs $MRI_{POST\text{-}2L}$	$MRI_{PRE\text{-}2C}$ vs $MRI_{PRE\text{-}2L}$	$MRI_{POST\text{-}1C}$ vs $MRI_{POST\text{-}1L}$	$MRI_{POST\text{-}2C}$ vs $MRI_{POST\text{-}2L}$
Geometric parameters	A_d	0.2042	0.9044	0.0027	0.2230	0.4912	0.3702	0.0157
	A_c	0.0545	0.0247	**	0.0056	0.0332	***	0.3373
	A_{sas}	*	0.0036	0.0175	0.2675	0.6254	0.3090	0.0612
	P_d	0.0377	0.9536	*	0.0512	0.0170	0.3940	0.2902
	P_c	0.6221	0.9015	0.0063	**	0.3013	0.0055	0.5454
	P_{sas}	****	0.1155	****	***	0.0034	0.0012	***
Hydrodynamic parameters	D_h	****	****	****	****	0.3255	0.5997	0.0080
	α	****	****	****	****	0.0565	****	0.1960
	Re	****	****	****	****	****	**	****
	$U_{peak\text{-}sys}$	****	****	****	****	****	0.0873	****
	$U_{peak\text{-}dia}$	****	****	****	****	0.0299	0.0008	****
	Q_a	****	****	****	****	****	*	****
	SV	****	****	****	****	****	0.0026	****

P: Probability value based on linear mixed effects model. The significance codes below use Bonferroni correction.
$p<0.05/91$ = *, $p<0.01/91$ = **, $p<0.005/91$ = ***, $p<0.001/91$ = ****

https://doi.org/10.1371/journal.pone.0244090.t003

$MRI_{POST\text{-}1C}$ and $MRI_{POST\text{-}2C}$ was markedly smaller than both $MRI_{PRE\text{-}2C}$ and $_{2L}$, and $MRI_{POST\text{-}1L}$ and $MRI_{POST\text{-}2L}$ due to catheter placement within cervical SAS in those cases.

Average spatial-temporal distribution of the CSF flow along the spine showed a relatively smooth decrease in amplitude with a caudally directed CSF pulse wave velocity (Fig 5). Pulse wave velocity magnitude was similar across the groups and ranged from 1.09–1.24 m/s. Maximum CSF flow rate occurred for the $MRI_{PRE\text{-}2}$ measurement within the cervical spine. Catheter placement decreased the flow rate spatially and temporally below the catheter tip in both $MRI_{POST\text{-}1}$ and $MRI_{POST\text{-}2}$.

Maximum *Re* number for $MRI_{PRE\text{-}2C}$ was 80 at C3-C4 level (Fig 6A). $MRI_{POST\text{-}2C}$ had the lowest *Re* value of 28 due to the cervical catheter implantation. Maximum Re_{NR}, Re_{δ} and Keulegan–Carpenter number was 12.55, 14.31 and 5.12 ($\beta = 2.79$), respectively. Catheter implantation also decreased CSF flow rate amplitude (Fig 6B) and stroke volume (Fig 6C) at $MRI_{POST\text{-}1C}$ and $MRI_{POST\text{-}2C}$ compared to $MRI_{PRE\text{-}2C}$ and for $MRI_{POST\text{-}1L}$ and $MRI_{POST\text{-}2L}$ compared to $MRI_{PRE\text{-}2L}$. Albeit, the changes in flow rate amplitude and stroke volume were greater under cervical implantation.

D_h (Fig 6D) and α (Fig 6E) decreased a great degree with cervical catheter implantation and to a lesser degree with lumbar implantation. Maximum D_h and α was 4 and 8 located near the FM. The peak value of the mean velocity ranged from +1.8 to -2.9 cm/s in $MRI_{PRE\text{-}2}$ and occurred at the C3-C4 level (Fig 6F). Based on Hagen–Poiseuille equation, CSF flow reduction was predicted to be 48% after cervical implantation and 6% after lumbar implantation. These predictions were comparable to the MRI-measured $Q_{peak\text{-}sys}$ reduction of 55% after cervical implantation and 21% after lumbar implantation (Table 2).

Discussion

To the best of our knowledge, the impact of intrathecal catheter implantation on spinal CSF dynamics in a cynomolgus monkey has not been reported in the literature. Our results showed

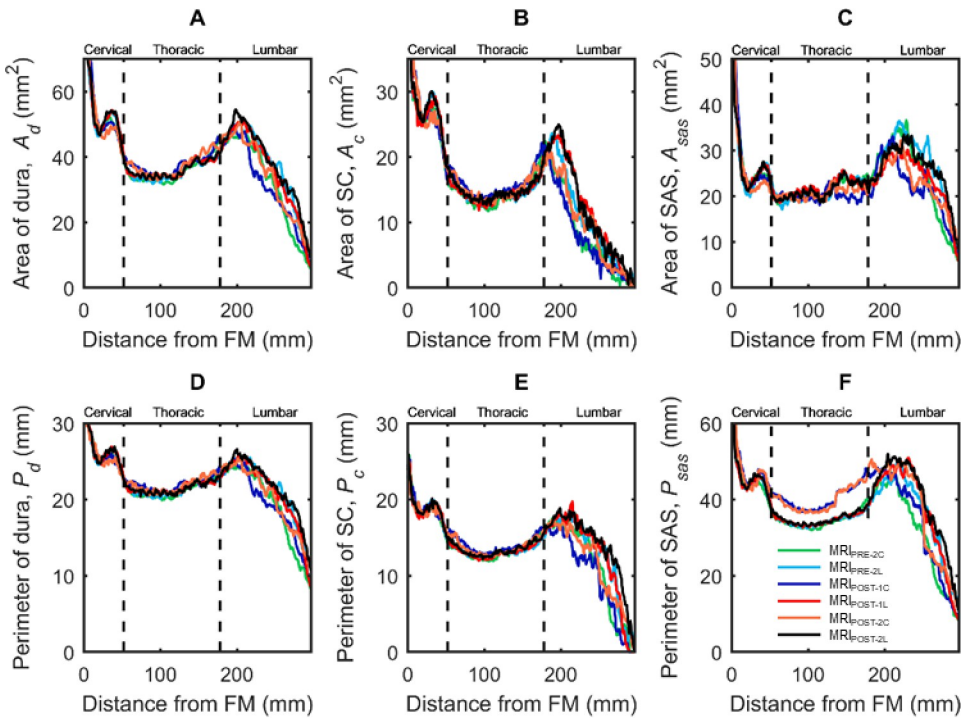

Fig 3. Axial distribution of geometric parameters computed along the spine for cynomolgus monkeys with cervical catheter implantation (MRI #C) or lumbar catheter implantation (MRI #L) was measured prior to catheter implantation (MRI_{PRE-2}), 17 days after catheter implantation (MRI_{POST-1}), and 31 days after catheter implantation (MRI_{POST-2}). (A) Area of dura, A_d, (B) Area of spinal cord, A_c, (C) Area of SAS, A_{sas}, (D) Perimeter of dura, P_d, (E) Perimeter of spinal cord, P_c, (F) Perimeter of SAS, P_{sas}. Each line corresponds to mean value of each NHPs group with catheter located in the lumbar (L) or cervical (c) spine before (MRI_{PRE-2}) or after catheter placement (MRI_{POST-1} and MRI_{POST-2}).

https://doi.org/10.1371/journal.pone.0244090.g003

that catheter implantation decreases spinal CSF dynamics and that the reduction was greater for cervical implantation compared to lumbar implantation. Also, that the decrease in spinal CSF dynamics was present immediately post-implantation and persisted two weeks after implantation. The MRI method used in this study to quantify intrathecal CSF dynamics in cynomolgus NHPs can be used to quantify intrathecal CSF dynamics and geometry in people with neurological disorders or healthy conditions. The technique provided for hydrodynamic parameter analysis could also aid development of emerging CSF deliverable therapeutics and be applied to better understand CSF-related pathologies.

Catheter insertion decreased spinal CSF flow

The potential impact of catheter implantation on intrathecal CSF dynamics should be considered when implanting spinal catheters in NHPs and potentially humans. Although catheter diameter was relatively small, our results showed that cervical catheter implantation reduced peak CSF flow by 55% compared to 21% for lumbar implantation (**Figs** 4 and 5). Additionally, nearly all measures of CSF dynamics were altered to a greater degree for cervical implantation compared to lumbar implantation (Table 2). These results were further supported by estimation of CSF flow reduction, based on the Hagen-Poiseuille equation, indicating that the CSF flow reduction was likely due to increased hydraulic resistance stemming from the catheter's reduction in SAS hydraulic diameter (Fig 3 and Table 2).

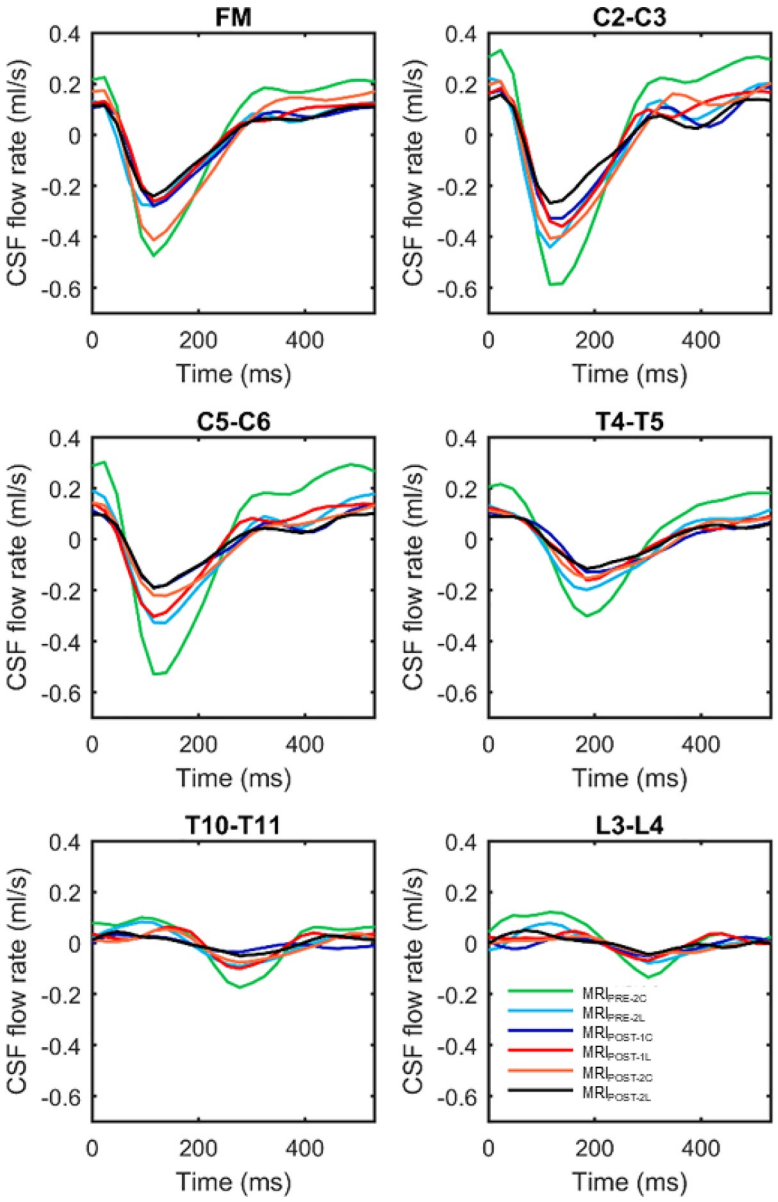

Fig 4. Average CSF flow waveforms for each MRI time point (4 NHPs at each point) measured at six axial locations along the spine (FM, C2-C3, C5-C6, T4-T5, T10-T11, L3-L4). Note: Peak systolic, CSF flow is in the caudal direction (negative values).

https://doi.org/10.1371/journal.pone.0244090.g004

Previous researchers have found that there has been a small possibility for infections or inflammatory conditions post-catheter insertion because of the reduction in CSF flow [29]. However, given that a) the reduction in CSF flow remained weeks following catheter insertion, b) the magnitude of flow reduction agreed with the estimated reduction based on fluid physics, and c) CSF flow reduction was greater for cervical catheter insertion, we believe the most probable source of CSF flow reduction to be increased hydraulic resistance directly due to the catheter.

In combination, the results indicate that to preserve normative intrathecal CSF flow, catheter placement should be located within the shortest length of the spine as possible and / or catheter diameter should be minimized to reduce its potential impact on hydraulic resistance

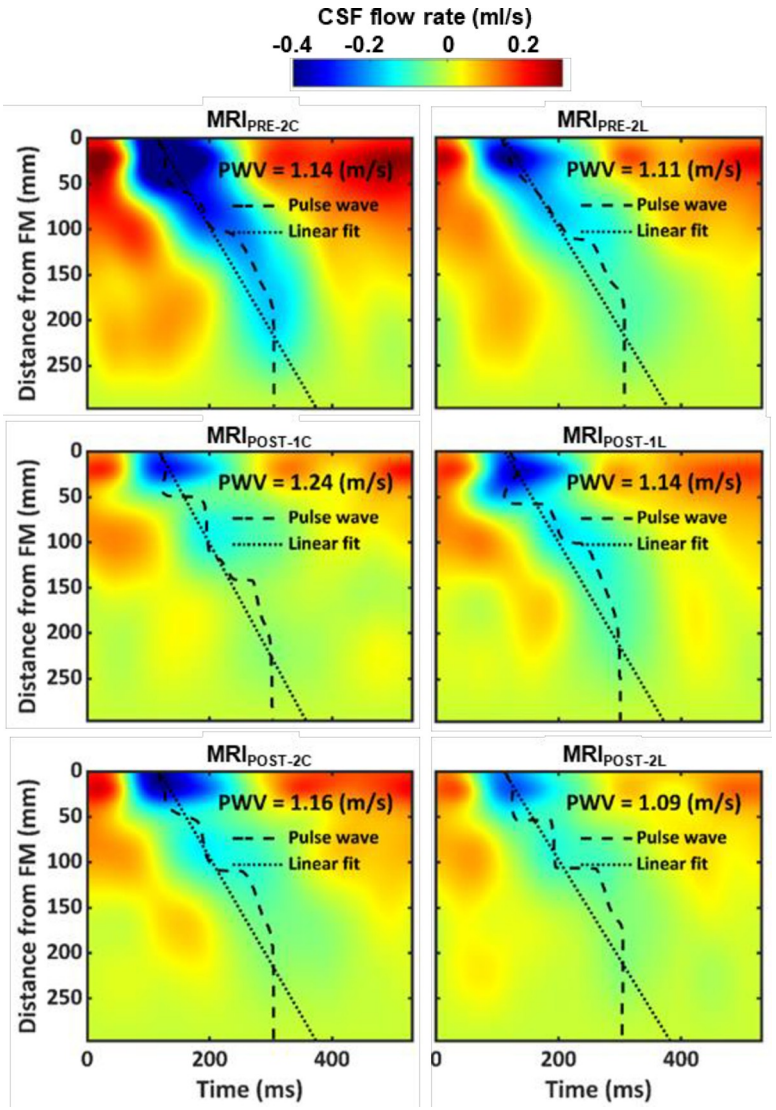

Fig 5. Mean CSF flow waveforms and Spatial-temporal distribution of CSF flow rate. Spatial-temporal distribution of the interpolated CSF flow rate along the spine for all cases measured by PC-MRI. Dashed line indicates peak CSF flow rate at each axial level and dotted line indicates linear fit on top of those values used to compute CSF pulse wave velocity (*PWV*).

https://doi.org/10.1371/journal.pone.0244090.g005

within the spinal SAS. However, a smaller diameter catheter may not allow infusion of a desired flow rate, which could potentially produce a flow jet near the catheter tip. These factors could be assessed by parametric simulations. Alternatively, if possible, lumbar puncture should be applied as it would have minimal impact on CSF hydraulic resistance within the spine in NHPs or humans. However, for prolonged intrathecal drug delivery applications, catheter insertion may be the only viable option for chronic drug delivery.

The distribution of CSF flow along the spine was non-uniform and showed local variations in waveform shape and magnitude at each axial location (Fig 4). For example, the CSF flow waveform amplitude was smaller at the FM compared to C2–C3 and then decreased at T4–T5 (Fig 4). CSF flow oscillations are primarily produced from cardiac-related pulsation of the intracranial arteries [30–32] and these collective pulsations result in oscillatory movement of CSF out of the cranial vault through the FM. The CSF flow pulse then travels down the spine

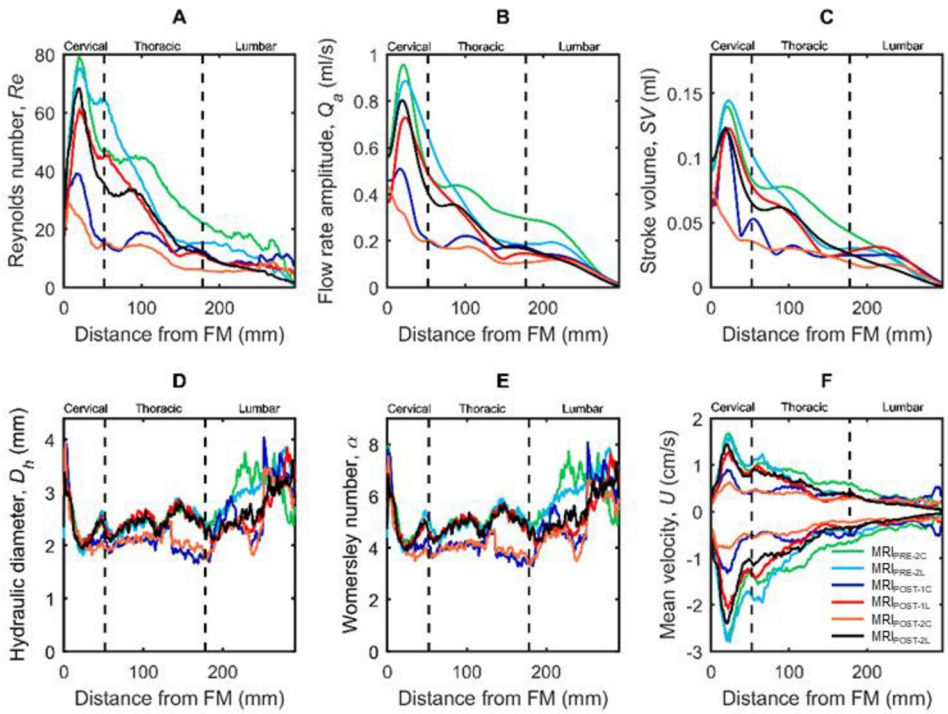

Fig 6. Hydrodynamic parameter axial distribution computed along the spine for cynomolgus monkeys. (A) Reynolds number, *Re*, (B) Flow rate amplitude, Q_a, (C) Stroke Volume, *SV*, (D) left axis, Hydraulic diameter, D_h, right axis, Womersley number, α, (E) mean peak systolic, $\bar{U}_{sys}$, and diastolic, $\bar{U}_{dia}$, CSF velocity. Each line corresponds to mean value of each NHPs group with catheter located in the lumbar or cervical spine before or after catheter placement.

https://doi.org/10.1371/journal.pone.0244090.g006

in a decreasing manner until its termination at the thecal sac. A numerical study has been done previously by our group indicates that a maximum radial dura displacement of ∼135 μm can satisfy mass conservation and reproduce the non-uniform CSF flow rates along the NHP spine. However, the radial motion of the dura has not been directly measured along the spine using MR imaging, likely due to the relatively small degree of motion present in that tissue.

Average *PWV* was found to be 1.15 m/s across all NHPs and was not impacted by catheter implantation (Fig 5). This is a potential indicator that spinal compliance, and likely intracranial pressure, was not affected due to catheter implantation. CSF *PWV* was previously measured by our research group in NHPs and found to have a similar value at 1.13 m/s [21]. However, in humans, CSF *PWV* was measured to be 1.94 m/s [33], indicating that *PWV* within the spine in humans to potentially be different than NHPs.

Spinal NHP CSF dynamics were laminar and inertial dominated

CSF flow remained laminar throughout the CSF flow cycle for all cases analyzed. Results showed that CSF dynamics were affected the most in the cervical spine near the C5 vertebral level in $MRI_{POST-2C}$ with a maximum *Re* of 28, 100% less than MRI_{PRE-2C} (Fig 6). Re_δ, was less than 14.31, which is below the threshold of 550 for conditional turbulence in oscillatory flow [34]. Appearance of instabilities in oscillatory flow around cylinders have been documented in a number of experiments for large β and small *K*, and the critical Keulegan–Carpenter number for these limits has been calculated as: $K_{cr} = 5.778\beta^{-1/4}(1+0.205\beta^{-1/4})$ given by Hall [28]. Thus,

for the current results, for which $\beta = 2.79$, K_{cr} has a value of 22.32. The value for the current results, $K = 5.12$, is below this threshold. Therefore, the occurrence of Honji-type instabilities [27] in the SAS are not expected. *Re* was computed to represent the ratio of steady inertial forces to viscous forces and help indicate whether laminar flow (<2300) was present at each phase-contrast slice location (**Fig 2**). A laminar CSF flow indicates that the flow is smooth with relatively little lateral mixing. This is different from a turbulent flow, where chaotic changes in pressure and velocity occur and can lead to a large increase in lateral mixing. Chaotic CSF velocity or pressure fluctuations are not expected to occur before or after catheter placement. However, it is possible that disease states that result in strongly elevated CSF flow velocities (jets) could result in turbulence [35].

Inertial effects are expected to dominate the SAS CSF flow field for normal physiological flow rates, frequencies and CSF fluid properties. α varied along the spine in a similar fashion as D_h with a minimum and maximum value of 3.8 and 8.1 (**Fig 6**). α was computed to quantify the ratio of unsteady inertial forces to viscous forces that impact the CSF velocity profile shape [36]. For $\alpha<2$, the CSF velocity profiles will be parabolic in shape and considered quasi-static. For $2<\alpha<10$ velocity profiles will be M-shaped and, for $\alpha>10$, velocity profiles will be relatively flat (plug shaped) [37]. The maximum value of α in the thoracic region decreased to ~4 after cervical catheter insertion. This concept implies that the CSF velocity profiles will show an M-shape throughout the spine. However, the upper cervical and lumbar spine had higher α indicating a relatively flat velocity profile within those regions. Our previous computational fluid dynamics NHP model without catheter implantation indicated a relatively blunt CSF velocity profile in the cervical spine [38]. It was not possible to confirm if the in vivo velocity profiles measured in the current study were blunt shaped (**Fig 2C**) as the MRI resolution was not fine enough to accurately capture the relatively thin boundary layer expected in a blunt or M-shaped flow profile.

Potential relevance of results with respect to intrathecal drug delivery

Based on the statistical analysis, catheter implantation led to decreased CSF flow rate within the spinal SAS, most notably under cervical implantation. In principle, a lower CSF flow rate is expected to decrease solute transport in the spine. Thus, we predicted that cervical catheter implantation would decrease solute transport to a greater degree than lumbar implantation. However, previous research [21], and our current study results (*Re* in **Fig 6A** and **Table 2**), indicate that CSF velocities and streaming in the cervical spine were much greater than the lumbar spine. Thus, although catheter placement in the cervical spine could result in decreased CSF flow, drug delivery in this region may still allow more rapid mixing compared to the lumbar spine. Catheter implantation location may also need to be taken into account alongside potentially diminished CSF flow dynamics in healthy [39] or disease states, such as amyotropic lateral sclerosis [11]. Optimal catheter implantation location can be explored in future work in combination with the potential role of catheter implantation on CSF flow dynamics, but was outside the scope of the present research.

Based on the results, it can be hypothesized that the impact of catheter implantation on CSF dynamics would potentially be greater in cynomolgus monkeys compared to adult humans due to relatively smaller SAS cross-sectional area in NHPs compared to humans (10X greater [11, 21]). The average catheter diameter of 1.5 mm used in this study for cynomolgus monkeys is within the range of catheter diameters used in humans, ranging from 1.2 to 1.65 mm in outer diameter [40]. Given the relatively smaller catheter diameter applied in adult humans, the potential impact of catheter implantation on CSF flow dynamics in adult humans may be relatively small. However, greater potential for catheter impact on CSF flow dynamics may be

present in pediatric humans due to their relatively smaller SAS cross-sectional area compared to adults.

Limitations and future directions

This study provides quantitative measures to investigate the impact of catheter insertion on intrathecal CSF dynamics and geometry in cynomolgus monkeys. Further studies should quantify the potential variance of these parameters in a larger study size across NHP species, in addition to including more diverse variables such as age, sex, weight, and disease states. Geometric characterization did not take into account spinal cord nerve root surface area or volume, which may account for ~231 cm^2 and ~6 ml, respectively within the SAS in humans [33]. It was expected that these structures may alter the SAS surface area results presented in the current study. Albeit, the surface area in contact with the spinal cord and dura was likely similar since the junction of spinal cord nerve roots with these structures is relatively small. Also, we did not expect these structures to alter the spinal cord and dura surface area to a great degree or total SAS volume.

There were also a few limitations in relation to CSF flow dynamics. First, CSF flow coupling with the cardiovascular cycle was accounted for in the present study. However, CSF flow has been shown to be impacted by respiration under normal breathing, forced breathing, and other maneuvers [41], which was not considered in this study using cardiac-gated PC-MRI measurements. This was because acquisition of the CSF respiration flow wave form would require a different MRI protocol that was not available on the MRI system utilized in this research. Future studies could investigate the relative contribution of respiration and cardiovascular pulsations to CSF flow dynamics along the spinal axis.

Catheter implantation may have had an impact on CSF production and/or absorption rate. Unfortunately, this study did not measure CSF production and/or absorption and, we are therefore unable to make any conclusion about this potential impact. Finally, CSF flow was measured at six axial locations and interpolated to generate a smooth distribution along the spine. The ideal study would minimize or eliminate interpolation as much as possible by adding more axial slice locations. CSF dynamics should also be quantified within the intracranial space to better understand the exact distribution of CSF flow disruption that a spinal catheter may produce. However, the MRI time limitation for each NHP did not allow more slice measurement locations. The focus of the present study was on the intrathecal space because this region is commonly accessed by lumbar puncture or other relatively minimally invasive procedures for drug delivery to the central nervous system. Injection of medications within the ventricular space of the brain or cortical SAS would also be impacted by nearby CSF dynamics within the ventricles and cisterns of the brain.

The axial distribution for all geometric parameters tended to have a similar trend (**Fig 3**) indicating a strong dependence among geometric parameters. This means that if one parameter shows a significant difference between two conditions or two-time points, some of the other parameters should also display a significant difference. On the other hand, if only one parameter shows a significant difference, such significance may be due to experimental error and may not be reliable. Therefore, although nine of the 42 p values in **Table 3** are significant, they are not consistent with the dependence among the parameters and therefore should be interpreted with caution.

Conclusions

This study presents a detailed geometric and hydrodynamic characterization of intrathecal CSF dynamics for eight cynomolgus monkeys (Macaca fascicularis) to quantify the differences

that occur based on catheter implantation location in the cervical compared to the lumbar spine. The overall findings were: 1) catheter insertion decreases CSF dynamics within the spine, 2) changes in CSF dynamics were greater for cervical implantation compared to lumbar catheter implantation, and 3) decrease in CSF dynamics persisted up to two weeks post-catheter implantation. In combination, these results support that intrathecal catheter implantation can adversely impact CSF flow dynamics in the spinal SAS in cynomolgus monkeys.

Supporting information

S1 Table. Source data for the axial distribution of SAS geometric and hydrodynamic parameters and the CSF flow waveforms collected at different vertebral levels. Data for all eight NHPs measured before catheter implantation ($MRI_{PRE\text{-}2}$) and after catheter implantation ($MRI_{POST\text{-}1}$ and $MRI_{POST\text{-}2}$).
(XLSX)

S1 File.
(DOCX)

Author Contributions

Conceptualization: Gregory R. Stewart, Bryn A. Martin.

Data curation: John N. Oshinski, Gregory R. Stewart, Jillynne R. Zeller, Bryn A. Martin.

Formal analysis: Bryn A. Martin.

Funding acquisition: Bryn A. Martin.

Investigation: Mohammadreza Khani, Bryn A. Martin.

Methodology: Mohammadreza Khani, Audrey Q. Fu, Joshua Pluid, Christina P. Gibbs, Tao Xing, Bryn A. Martin.

Project administration: Bryn A. Martin.

Resources: Bryn A. Martin.

Software: Bryn A. Martin.

Supervision: Bryn A. Martin.

Validation: Mohammadreza Khani, Bryn A. Martin.

Visualization: Mohammadreza Khani, Bryn A. Martin.

Writing – original draft: Mohammadreza Khani, Audrey Q. Fu, Joshua Pluid, Christina P. Gibbs, John N. Oshinski, Bryn A. Martin.

Writing – review & editing: Mohammadreza Khani, Audrey Q. Fu, John N. Oshinski, Tao Xing, Gregory R. Stewart, Jillynne R. Zeller, Bryn A. Martin.

References

1. Upadhyay SP, Mallick PN. Intrathecal drug delivery system (IDDS) for cancer pain management: a review and updates. Am J Hosp Palliat Care. 2012; 29(5):388–98. https://doi.org/10.1177/1049909111426134 PMID: 22089523
2. McCall TD, MacDonald JD. Cervical catheter tip placement for intrathecal baclofen administration. Neurosurgery. 2006; 59(3):634–40; discussion -40. https://doi.org/10.1227/01.NEU.0000227570.40402.77 PMID: 16955045

3. Schorling DC, Pechmann A, Kirschner J. Advances in Treatment of Spinal Muscular Atrophy—New Phenotypes, New Challenges, New Implications for Care. J Neuromuscul Dis. 2020; 7(1):1–13. https://doi.org/10.3233/JND-190424 PMID: 31707373

4. Figura NB, Rizk VT, Armaghani AJ, Arrington JA, Etame AB, Han HS, et al. Breast leptomeningeal disease: a review of current practices and updates on management. Breast Cancer Res Treat. 2019; 177 (2):277–94. https://doi.org/10.1007/s10549-019-05317-6 PMID: 31209686

5. Ejikeme T, de Castro GC, Ripple K, Chen Y, Giamberardino C, Bartuska A, et al. Evaluation of neurapheresis therapy in vitro: a novel approach for the treatment of leptomeningeal metastases. Neurooncol Adv. 2020; 2(1):vdaa052. https://doi.org/10.1093/noajnl/vdaa052 PMID: 32642705

6. Khani M, Sass L, McCabe A, Zitella Verbick L, Lad SP, Sharp MK, et al. Impact of Neurapheresis system on intrathecal cerebrospinal fluid dynamics: a computational fluid dynamics study. J Biomech Eng. 2019. https://doi.org/10.1115/1.4044308 PMID: 31343659

7. Smilnak GJ, Charalambous LT, Cutshaw D, Premji AM, Giamberardino CD, Ballard CG, et al. Novel Treatment of Cryptococcal Meningitis via Neurapheresis Therapy. J Infect Dis. 2018; 218(7):1147–54. https://doi.org/10.1093/infdis/jiy286 PMID: 29788431

8. Sanchez AL, Martinez-Bazan C, Gutierrez-Montes C, Criado-Hidalgo E, Pawlak G, Bradley W, et al. On the bulk motion of the cerebrospinal fluid in the spinal canal. Journal of Fluid Mechanics. 2018; 841:203–27.

9. Tangen K, Nestorov I, Verma A, Sullivan J, Holt RW, Linninger AA. In Vivo Intrathecal Tracer Dispersion in Cynomolgus Monkey Validates Wide Biodistribution Along Neuraxis. IEEE Trans Biomed Eng. 2020; 67(4):1122–32. https://doi.org/10.1109/TBME.2019.2930451 PMID: 31352328

10. Brinker T, Stopa E, Morrison J, Klinge PJF, CNS Bot. A new look at cerebrospinal fluid circulation. 2014; 11(1):10.

11. Sass LR, Khani M, Romm J, Schmid Daners M, McCain K, Freeman T, et al. Non-invasive MRI quantification of cerebrospinal fluid dynamics in amyotrophic lateral sclerosis patients. Fluids Barriers CNS. 2020; 17(1):4. https://doi.org/10.1186/s12987-019-0164-3 PMID: 31959193

12. Baledent O, Henry-Feugeas MCC, Idy-Peretti I. Cerebrospinal fluid dynamics and relation with blood flow—A magnetic resonance study with semiautomated cerebrospinal fluid segmentation. Investigative Radiology. 2001; 36(7):368–77. https://doi.org/10.1097/00004424-200107000-00003 PMID: 11496092

13. Aktas G, Kollmeier JM, Joseph AA, Merboldt KD, Ludwig HC, Gartner J, et al. Spinal CSF flow in response to forced thoracic and abdominal respiration. Fluids Barriers CNS. 2019; 16(1):10. https://doi.org/10.1186/s12987-019-0130-0 PMID: 30947716

14. Yamada S, Miyazaki M, Yamashita Y, Ouyang C, Yui M, Nakahashi M, et al. Influence of respiration on cerebrospinal fluid movement using magnetic resonance spin labeling. Fluids Barriers CNS. 2013; 10 (1):36. https://doi.org/10.1186/2045-8118-10-36 PMID: 24373186

15. Snead OC 3rd, LaCroix JT. Lumbar puncture for obtaining cerebrospinal fluid in the rhesus monkey (Macaca mulatta). Lab Anim Sci. 1977; 27(6):1039–40. PMID: 414022

16. Butler TM, Wiley GL. Baseline values for adult baboon cerebrospinal fluid. Lab Anim Sci. 1971; 21 (1):123–4. PMID: 4322774

17. Derwellis SK, Butler TM, Fineg J. Baseline values of cerebrospinal fluid from the chimpanzee (Pan troglodytes). Lab Anim Care. 1970; 20(1):107–8. PMID: 4244715

18. Turbyfill CL, Cramer MB, Dewes WA, Huguley JW 3rd. Serum and cerebral spinal fluid chemistry values for the monkey (Macaca mulatta). Lab Anim Care. 1970; 20(2):269–73. PMID: 4315781

19. Taylor PL, Garrick NA, Burns RS, Tamarkin L, Murphy DL, Markey SP. Diurnal rhythms of serotonin in monkey cerebrospinal fluid. Life Sci. 1982; 31(18):1993–9. https://doi.org/10.1016/0024-3205(82)90038-8 PMID: 7176807

20. Tangen KM, Leval R, Mehta AI, Linninger AA. Computational and in vitro experimental investigation of intrathecal drug distribution: parametric study of the effect of injection volume, cerebrospinal fluid pulsatility, and drug uptake. Anesthesia & Analgesia. 2017; 124(5):1686–96.

21. Khani M, Lawrence BJ, Sass LR, Gibbs CP, Pluid JJ, Oshinski JN, et al. Characterization of intrathecal cerebrospinal fluid geometry and dynamics in cynomolgus monkeys (macaca fascicularis) by magnetic resonance imaging.(Research Article)(Report). PLoS ONE. 2019; 14(2):e0212239. https://doi.org/10.1371/journal.pone.0212239 PMID: 30811449

22. Yushkevich PA, Piven J, Hazlett HC, Smith RG, Ho S, Gee JC, et al. User-guided 3D active contour segmentation of anatomical structures: significantly improved efficiency and reliability. Neuroimage. 2006; 31(3):1116–28. https://doi.org/10.1016/j.neuroimage.2006.01.015 PMID: 16545965

23. Kalata W, Martin BA, Oshinski JN, Jerosch-Herold M, Royston TJ, Loth F. MR Measurement of Cerebrospinal Fluid Velocity Wave Speed in the Spinal Canal. IEEE transactions on bio-medical engineering. 2009. https://doi.org/10.1109/TBME.2008.2011647 PMID: 19174343

24. Yiallourou TI, Kroger JR, Stergiopulos N, Maintz D, Martin BA, Bunck AC. Comparison of 4D phase-contrast MRI flow measurements to computational fluid dynamics simulations of cerebrospinal fluid motion in the cervical spine. PLoS One. 2012; 7(12):e52284. https://doi.org/10.1371/journal.pone.0052284 PMID: 23284970

25. Martin BA, Kalata W, Shaffer N, Fischer P, Luciano M, Loth F. Hydrodynamic and longitudinal impedance analysis of cerebrospinal fluid dynamics at the craniovertebral junction in type I Chiari malformation. PLoS One. 2013; 8(10):e75335. https://doi.org/10.1371/journal.pone.0075335 PMID: 24130704

26. Darian-Smith C. Monkey models of recovery of voluntary hand movement after spinal cord and dorsal root injury. ILAR J. 2007; 48(4):396–410. https://doi.org/10.1093/ilar.48.4.396 PMID: 17712225

27. Honji H. Streaked Flow around an Oscillating Circular-Cylinder. J Fluid Mech. 1981; 107(Jun):509–20.

28. Hall P. On the Stability of the Unsteady Boundary-Layer on a Cylinder Oscillating Transversely in a Viscous-Fluid. J Fluid Mech. 1984; 146(Sep):347–67.

29. McLaurin RL, Frame PT. Treatment of infections of cerebrospinal fluid shunts. Rev Infect Dis. 1987; 9 (3):595–603. https://doi.org/10.1093/clinids/9.3.595 PMID: 3602797

30. Rennels ML, Gregory TF, Blaumanis OR, Fujimoto K, Grady PA. Evidence for a Paravascular Fluid Circulation in the Mammalian Central Nervous-System, Provided by the Rapid Distribution of Tracer Protein Throughout the Brain from the Subarachnoid Space. Brain Res. 1985; 326(1):47–63. https://doi.org/10.1016/0006-8993(85)91383-6 PMID: 3971148

31. Stoodley MA, Brown SA, Brown CJ, Jones NR. Arterial pulsation-dependent perivascular cerebrospinal fluid flow into the central canal in the sheep spinal cord. Journal of Neurosurgery. 1997; 86(4):686–93. https://doi.org/10.3171/jns.1997.86.4.0686 PMID: 9120633

32. Hadaczek P, Yamashita Y, Mirek H, Tamas L, Bohn MC, Noble C, et al. The "perivascular pump" driven by arterial pulsation is a powerful mechanism for the distribution of therapeutic molecules within the brain. Mol Ther. 2006; 14(1):69–78. https://doi.org/10.1016/j.ymthe.2006.02.018 PMID: 16650807

33. Sass LR, Khani M, Natividad GC, Tubbs RS, Baledent O, Martin BA. A 3D subject-specific model of the spinal subarachnoid space with anatomically realistic ventral and dorsal spinal cord nerve rootlets. Fluids Barriers CNS. 2017; 14(1):36. https://doi.org/10.1186/s12987-017-0085-y PMID: 29258534

34. Hino M, Sawamoto M, Takasu S. Experiments on Transition to Turbulence in an Oscillatory Pipe-Flow. J Fluid Mech. 1976; 75(May27):193–207.

35. Jain K, Ringstad G, Eide PK, Mardal KA. Direct numerical simulation of transitional hydrodynamics of the cerebrospinal fluid in Chiari I malformation: The role of cranio-vertebral junction. International Journal for Numerical Methods in Biomedical Engineering. 2017; 33(9). https://doi.org/10.1002/cnm.2853 PMID: 27863152

36. Loth F, Yardimci MA, Alperin N. Hydrodynamic modeling of cerebrospinal fluid motion within the spinal cavity. J Biomech Eng. 2001; 123(1):71–9. https://doi.org/10.1115/1.1336144 PMID: 11277305

37. Khani M, Sass LR, Xing T, Keith Sharp M, Balédent O, Martin BA. Anthropomorphic Model of Intrathecal Cerebrospinal Fluid Dynamics Within the Spinal Subarachnoid Space: Spinal Cord Nerve Roots Increase Steady-Streaming. Journal of Biomechanical Engineering. 2018; 140(8):081012–15. https://doi.org/10.1115/1.4040401 PMID: 30003260

38. Khani M, Xing T, Gibbs C, Oshinski JN, Stewart GR, Zeller JR, et al. Nonuniform Moving Boundary Method for Computational Fluid Dynamics Simulation of Intrathecal Cerebrospinal Flow Distribution in a Cynomolgus Monkey. J Biomech Eng. 2017; 139(8).

39. Eklund A, Koskinen LOD, Malm J. Features of the Sinushunt (R) and its influence on the cerebrospinal fluid system. J Neurol Neurosur Ps. 2004; 75(8):1156–9.

40. Nagel SJ, Reddy CG, Frizon LA, Holland MT, Machado AG, Gillies GT, et al. Intrathecal Therapeutics: Device Design, Access Methods, and Complication Mitigation. Neuromodulation. 2018; 21(7):625–40. https://doi.org/10.1111/ner.12693 PMID: 28961351

41. Yildiz S, Thyagaraj S, Jin N, Zhong X, Heidari Pahlavian S, Martin BA, et al. Quantifying the influence of respiration and cardiac pulsations on cerebrospinal fluid dynamics using real-time phase-contrast MRI. J Magn Reson Imaging. 2017; 46(2):431–9. https://doi.org/10.1002/jmri.25591 PMID: 28152239